JCTC Journal of Chemical Theory and Computation

Design of a Versatile Force Field for the Large-Scale Molecular Simulation of Solid and Liquid OMCTS

Hiroki Matsubara,*,† Fabio Pichierri,*,† and Kazue Kurihara‡

G-COE Laboratory, Department of Applied Chemistry, Graduate School of Engineering, Tohoku University and JST-CREST, Aoba-yama 6-6-07, Sendai 980-8579, Japan, and Institute of Multidisciplinary Research for Advanced Materials (IMRAM), Tohoku University, JST-CREST, 2-1-1 Katahira, Sendai 980-8577, Japan

Received November 17, 2009

Abstract: We developed a new, versatile force field for the molecular simulation of octamethylcyclotetrasiloxane (OMCTS) both in the solid and liquid phases. From a series of molecular dynamics simulations, we obtain good agreement with the experimental lattice constants, sublimation enthalphy, and molecular packing of the crystal. The experimental density, diffusion coefficient, and shear viscosity of this van der Waals liquid in the range 300−440 K are well reproduced as well. The new force field can be thus employed in the large-scale molecular simulation of liquid OMCTS where structural details are important in determining the collective properties of the system.

I. Introduction

Octamethylcyclotetrasiloxane (OMCTS, Chart 1) is a small macrocycle made of four covalently linked $Si(Me)_2O$ units which has been used as a model liquid in surface force measurements (SFM).[1–7] These experiments have revealed the existence of oscillatory solvation forces which are characteristic of the behavior of liquids confined in nanosized spaces, and OMCTS, due to its quasi-spherical shape and zero dipole moment, has contributed to the development of theoretical treatments of these phenomena. In many cases, the molecular level origin of such phenomena is not clear from these experiments, and molecular simulation, particularly molecular dynamics (MD) and Monte Carlo methods, is used to connect these phenomena with the behavior of molecular ensembles that are subject to confinement.[8–10]

Molecular simulation of real materials requires realistic potentials which are necessary to accurately describe the interactions among a large number of molecules.[11,12] Especially challenging is the design of intermolecular potentials concerned with weak dispersion interactions that operate among large molecules.[13] Flexible molecules further increase the complexity of the potential thereby making large-scale computations very demanding.

Chart 1

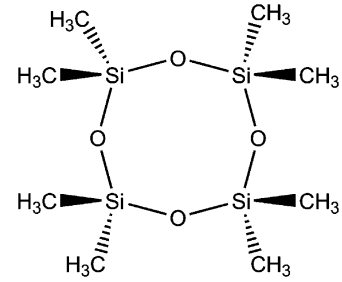

Possible alternative approaches that overcome system size are multiscale and coarse grain models.[14,15] The former are concerned with the integrated combination of different methodologies, from quantum mechanics up to the finite element method, each of which is appropriate to describe the system under study at different scales. Coarse grain (CG) methods on the other hand are used to simulate ensembles of large molecules each of which is modeled as a collection of beads rather than atoms. In this regard, Klein and coworkers have recently performed CG-MD simulations to investigate antimicrobial polymers and polypeptides.[16] Another difficulty encountered in the large-scale computations is concerned with the transferability of the interatomic or

* Corresponding author e-mail: fabio@che.tohoku.ac.jp (F.P.); matsubara@che.tohoku.ac.jp (H.M.).

† Graduate School of Engineering.

‡ IMRAM.

10.1021/ct9006053
Published on Web 03/01/2010

intermolecular potentials to different physical states of the system, namely condensed (solid and liquid) and vapor phases. Therefore, with a few exceptions,[17,18] the large majority of force fields are generally employed to study complex molecular systems that are in a specific phase while the study of different phases of the system usually requires using different sets of parameters.

So far, only simple spherical (or ellipsoidal) models are found in molecular simulation studies of OMCTS.[8–10] For instance, Ayappa and Mishra[10] have recently performed a series of grand canonical Monte Carlo simulations on spherical OMCTS molecules of diameter 7.7 Å and interacting with each other through a 12−6 Lennard-Jones (LJ) potential. While such models are useful for discussing phase transitions that occur under confinement, more desirable is the model that makes use of information contained in the molecular structure so that atomic-scale details on both molecular packing and specific intermolecular interactions can be gained from the simulations. To develop such a model is the main objective of this study.

The paper is structured as follows. In section II, we develop our original force field based on the assumption that the methyl−methyl (Me−Me) interaction is the dominant intermolecular interaction among OMCTS molecules. *Ab-initio* quantum mechanical (QM) calculations are employed to construct the potential energy surface corresponding to the interaction between methane molecules (CH_4). This intermolecular potential is expected to mimic the weak van der Waals (vdW) interactions that operate among the methyl groups of OMCTS molecules. We subsequently perform a series of classical MD simulations[11,12] to test the new potential and hence confirm our initial assumption. The potential is validated in section III by checking how accurately the crystal lattice constants, sublimation enthalpy (ΔH_{subl}), and liquid density (at 300 and 400 K) are reproduced. In section IV, the force field is further refined by employing a penalty function which depends on the lattice constants, ΔH_{subl}, and the density of the liquid at two different temperatures. In section V, the refined force field is then employed in a long MD simulation of OMCTS liquid, and the calculated bulk properties are compared against experimental data. Conclusions and remarks are given in section VI.

II. Potential Model

The OMCTS molecule has a disk-like shape and possesses eight methyl groups which are located at the outermost point while the atoms of the siloxane ring (Si and O) are well embedded inside the van der Waals (vdW) surface of the molecule, as shown in Figure 1. Besides shielding the siloxane ring from the outer environment, the methyl groups also confer overall conformational rigidity to the macrocyle owing to the increase in intramolecular steric repulsion. Because OMCTS is a neutral molecule with a negligible dipole moment ($\mu = 0.22$ D), dispersive interactions are likely the main components of the intermolecular interactions among OMCTS molecules. An inspection into the OMCTS crystal[19] indicates that the shortest intermolecular distance among non-hydrogen atoms is that between the carbon atoms

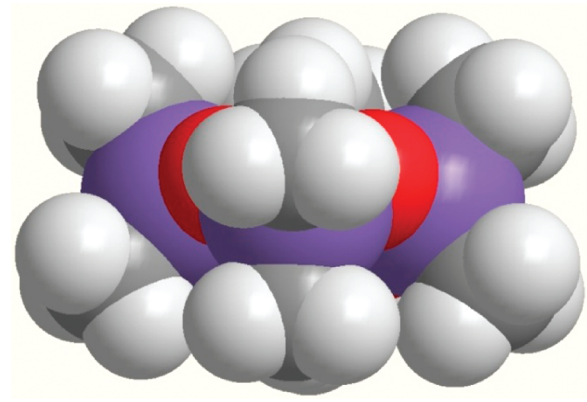

Figure 1. Space-filling representation of the OMCTS molecule.

of the methyl groups (C···C < 4.0 Å) while CH···HC contacts are in the range 2.3−3.0 Å, thereby supporting the above hypothesis. We therefore considered a model of the OMCTS molecule in which only Me−Me interactions are included. The molecule is assumed to be a rigid body whose geometry is taken from the molecular crystal.[19] One methyl group site is located on each carbon atom position, and hydrogen atoms were implicitly included. The interaction energy E_{ij} of a pair of methyl sites i and j in different molecules is described by the Lennard-Jones potential:

$$E_{ij} = 4\varepsilon\left[\left(\frac{\sigma}{r_{ij}}\right)^{12} - \left(\frac{\sigma}{r_{ij}}\right)^{6}\right] \quad (1)$$

where, r_{ij} is the distance between methyl sites. The parameters σ and ε were derived from a series of QM calculations performed on the methane dimer.

The quantum mechanical approach employed here is based on the second-order Møller−Plesset perturbation theory (MP2)[20] in combination with the 6-31G(d,p),[21] 6-311++G(2d,2p),[22] and AUG-cc-pVDZ[23] basis sets as implemented in the parallel version of the Gaussian 03 software package.[24] Early theoretical studies on the methane dimer have established that the lowest energy configuration arises from the face-to-face interaction between methane molecules in the D_{3d}-symmetric dimer.[25] By using this configuration, we first optimized the geometry of the dimer at the three levels of MP2 theory described above. The carbon−carbon distance in the optimized geometries of the dimer correspond to 3.804 Å at the MP2/6-31G(d,p) level, 3.803 Å at the MP2/6-311++G(2d,2p) level, and 3.575 Å at the MP2/AUG-cc-pVDZ level. Starting from these optimized geometries, we have computed the corresponding potential energy curves (PECs) by stepwise elongation and compression of the carbon−carbon distance while optimizing all the remaining degrees of freedom. From these calculations, we notice that only the PEC computed with the smaller 6-31G(d,p) basis set appears as a continuous curve, whereas those computed with the larger basis sets show a discontinuity in the repulsive part. This problem arises from the well-known basis set superposition error (BSSE)[26] which increases dramatically at $r(CC) < r(CC)_{eq}$. We have therefore computed the PECs by performing relaxed potential energy surface scans which were corrected at each step by using the counterpoise correction (CP) method of Boys and Bernardi.[27]

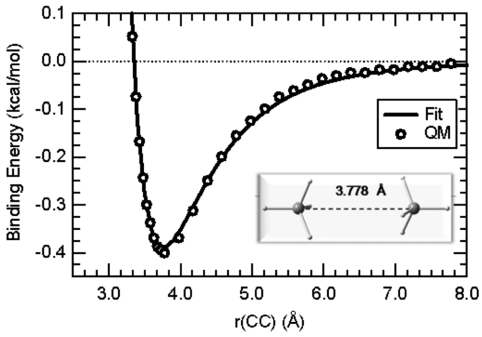

Figure 2. CP-corrected potential energy curve for the D_{3d}-symmetric methane dimer as computed at the MP2/AUG-cc-pVDZ level of theory. The inset shows the CP-corrected optimized geometry of the methane dimer.

The CP-corrected PEC of the methane dimer computed at the MP2/AUG-cc-pVDZ level of theory is shown in Figure 2. The minimum is located at $r(CC)_{eq} = 3.778$ Å, and the BSSE-corrected binding energy of the dimer corresponds to 0.402 kcal/mol. By fitting this PEC with the LJ function (eq 1), the parameters $\sigma = 3.35$ Å and $\varepsilon = 0.390$ kcal/mol were derived. This set of parameters is hereafter labeled as Model-A. In comparison, the CP-corrected geometry of the minimum computed at the MP2/6-311++G(2d,2p) level is located at $r(CC)_{eq} = 3.804$ Å. Also, we checked how the introduction of silicon affects $r(CC)_{eq}$ by considering the H_3C-SiH_3 molecule. The CP-corrected geometry of the $H_3Si-CH_3\cdots H_3C-SiH_3$ dimer obtained at the MP2/AUG-cc-pVDZ level of theory is characterized by $r(CC)_{eq} = 3.867$ Å, which is only 0.089 Å longer than the corresponding intermolecular carbon−carbon distance of the methane dimer. This small elongation of $r(CC)_{eq}$ can be attributed to the presence of repulsive dipole−dipole interactions ($\mu = 0.69$ D) that are operative in the H_3C-SiH_3 dimer with respect to the methane dimer where $\mu = 0$ D. Despite its simplicity, the methane dimer represents a good starting model for modeling the methyl−methyl interaction between two OMCTS molecules whose dipole moment is only 0.22 D (for the C_s-symmetric geometry optimized at the PBE1PBE/6-31G(d) level of theory).

III. Model Validation

The LJ parameters of Model-A were validated by performing MD simulations on both liquid and crystal phases. We utilized the DLPOLY2 (version 2.20) package[28] for all the MD simulations in this study. For the crystal phase, we executed simulations with a constant number of molecules, constant pressure, and constant temperature where the size and shape of the simulation box were allowed to change ($N\sigma T$ ensemble) by using the method of Berendsen et al.[29] The time constants used were 0.2 ps for the thermostat and 0.3 ps for the barostat. The simulation box contained 216 OMCTS molecules, and three-dimensional periodic boundary conditions (PBCs) were imposed. The cutoff radius for the vdw interactions was 20.0 Å. The time step was set to 2.0 fs. The velocity Verlet and NOSQUISH[30] algorithms were used for the numerical integration of the translational and rotational parts of the equation of motion. The temperature and total pressure were controlled to 223 K and 1 atm. The initial configuration was constructed by replicating the unit cell of the molecular crystal[19] so as to obtain a box of dimensions $A = 3a$, $B = 3b$, $C = 6c$. After a 40 ps run for equilibration, a statistical average was taken over 100 ps.

For the liquid phase, we executed simulations with a constant number of molecules, constant pressure, and constant temperature where only the cell size was allowed to vary (*NPT* ensemble) by using the method of Berendsen et al.[29] The time constants were the same as those of the crystal simulation. We considered the two different temperatures of 300 and 400 K which are close to the experimental melting and boiling temperatures of 290 and 444 K,[31] respectively. For all these cases, the pressure was set to 1 atm. The initial configuration was obtained from a random molecular configuration kept at a temperature of 1000 K for several tens of picoseconds while the simulation box was a cube of 48.3 Å. Subsequently, the system was quenched to the setting temperature of 300 or 400 K by rescaling the molecular velocities, and from this point on the box size was allowed to vary. The statistical average was taken over 200 ps after several tens of picoseconds for equilibration. Other conditions were the same as those employed in the simulation of the crystal. From these simulations, we calculated the lattice constants, a, b, and c; sublimation enthalpy, ΔH_{subl} (calculated here as the potential energy per molecule at 223 K); and liquid densities at 300 and 400 K, ρ_{300} and ρ_{400}. Those are compared with the experimental values reported in Table 1.

As can be noted, the performance of Model-A is fairly good with computed lattice constants that are slightly smaller than the corresponding experimental values and the computed ΔH_{subl} of −16 kcal/mol, which is close to the experimental value of −15.3 kcal/mol taken from ref 30. The space group of the experimental crystal ($P4_2/n$) was maintained during the whole simulation. The computed liquid densities at 300 and 400 K are also in satisfactory agreement with the experimental densities[31] at these temperatures.

Also, for comparison purposes, we executed similar simulations using different force fields. The DREIDING force field,[34] a general purpose force field, has an intermolecular LJ parameter for carbon with three implicit hydrogen atoms. If the methyl parameter of Model-A is replaced by this parameter, the lattice constants become closer to the experimental values, but the interaction energy is weakened, thus resulting in a liquid that possesses too low a density at 300 K (655 kg/m^3). On the other hand, at 400 K, these parameters give rise to a vapor phase. Interestingly, the properties computed by using the DREIDING all-atom (Si, O, Me) parameters worsen with respect to the methyl-only simulation, as seen in Table 1, where even at 400 K an amorphous solid structure resulted from the simulation. Further, we also examined the model of Smith et al.,[35] which has been designed for the simulation of poly dimethylsiloxane and uses the rigid body approximation (the molecular geometry of OMCTS used for this model was obtained from a geometry optimization using the Gaussian 03 program). This model, which includes both vdW and electrostatic interaction sites on all atoms, gave good results for the lattice

Table 1. Computed and Experimental Properties for Solid and Liquid OMCTS

property	Model-A	DREIDING (methyl only)	DREIDING (all atom)	Smith et al.	Model-B	expt.
a (Å)	15.33	16.2	15.6	16.24	15.73	16.10[a]
b (Å)	15.33	16.2	15.6	16.24	15.73	16.10[a]
c (Å)	6.01	6.86	6.07	6.63	6.23	6.47[a]
ΔH_{subl} (kcal/mol)	−16.0	−10.6	−33.6	−22.1	−16.9	−15.3[b]
ρ_{300} (kg/m^3)	1023	655	solid	solid	948	948[c]
ρ_{400} (kg/m^3)	801	vapor	solid	solid	790	830[c]

[a] Steinfink et al. (ref 19). [b] Osthoff et.al. (ref 32). [c] Palczewska-Tulińska and Oracz (ref 33).

constants, but like for the DREIDING (all atom) case, an amorphous solid was obtained for the liquid state. Hence, it appears that the attractive force between molecules becomes too large when the Si and O terms are added to the intermolecular potential.

In summary, our simulations indicate that Model-A describes quite well the properties of both crystal and liquid phases, thus confirming our assumption that the dominant intermolecular interaction in bulk OMCTS is that among the methyl groups. We also checked how the introduction of atomic charges affects our simulation results. We derived two sets of atomic charges from quantum mechanical calculations performed on the OMCTS molecule, one by fitting the electrostatic potential (ESP) and another by performing a standard Mulliken population analysis of the molecular wave function computed at the MP2/AUG-cc-pVDZ//PBE1PBE/6-31G(d) level of theory. Simulations indicate that including these atomic charges gives slightly shorter lattice constants than those obtained with Model-A, but no specific advantage was seen in spite of the larger computational cost due to the calculation of electrostatic interaction.

IV. Empirical Refinement

Our simulations indicate that Model-A possesses the essential features for describing the intermolecular interactions in OMCTS. However, because OMCTS is more complex a molecule than methane, there should be room for further refinement of this model. Therefore, we empirically readjusted the two LJ parameters of Model-A so as to reproduce the experimental data. We performed the same simulation as those in the previous section for a number of different parameter sets, among which the best set was chosen so as to minimize the penalty function F expressed as the sum of relative errors on the properties that are listed in Table 1:

$$F = f(a) + f(b) + f(c) + f(\Delta H_{subl}) + f(\rho_{300}) + f(\rho_{400}) \quad (2)$$

where $f(x)$ is defined as the relative percentage error of x:

$$f(x) = \left| \frac{x_{expt} - x_{calc}}{x_{expt}} \right| \times 100 \quad (3)$$

where x_{expt} and x_{calc} are the experimental and calculated values of x, respectively. Additionally, we excluded the parameter sets that did not produce a vapor phase at 500 K. Following this procedure, the best parameter set was determined as being $\sigma = 3.54$ Å and $\varepsilon = 0.39$ kcal/mol, which we define as Model-B. This pair of parameters is located at the bottom

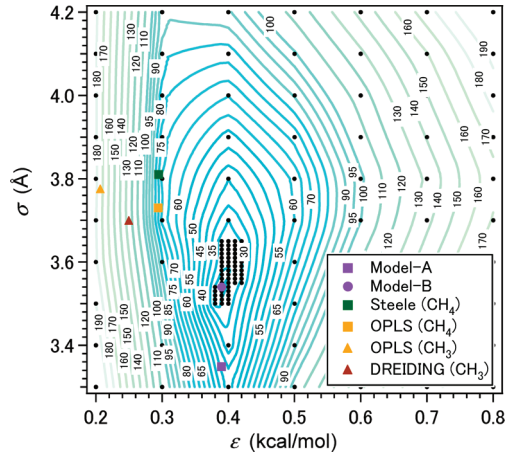

Figure 3. Contour plot of the penalty function F. The location of existing LJ parameters of methane (CH_4) and the methyl group (CH_3) are also plotted in this figure: $\sigma = 3.81$ Å and $\varepsilon = 0.294$ kcal/mol from Steele;[36] $\sigma = 3.73$ Å and $\varepsilon = 0.294$ kcal/mol from OPLS (CH_4);[37] $\sigma = 3.775$ Å and $\varepsilon = 0.207$ kcal/mol from OPLS (CH_3);[37] $\sigma = 3.7$ Å and $\varepsilon = 0.25$ kcal/mol from DREIDING (CH_3).[34]

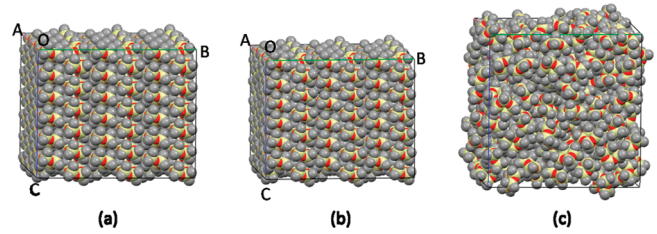

Figure 4. Comparison between (a) experimental and (b) computed OMCTS molecular crystal. (c) Snapshot of the OMCTS liquid. A cubic box was employed for the liquid simulation.

of the contour plot of the penalty function F shown in Figure 3. The coordinates of all the points used to make the contour plot are given in the Supporting Information (Table S1). For the purpose of comparison, the results obtained using Model-B are listed in Table 1.

Figure 4a,b shows the experimental and computed crystal unit cells of OMCTS. It is worth noticing that the simulated molecular crystal is characterized by the same type of packing as that of the experimental crystal where the molecules are stacked along the c axis and interact with each other using four methyl groups above and four below the molecular plane. A snapshot of the OMCTS liquid is shown in Figure 4c. Figure 5 shows the calculated radial distribution functions (RDFs) for intermolecular Me−Me pairs in both crystal (at 223 K) and liquid (at 300 and 400 K) simulations.

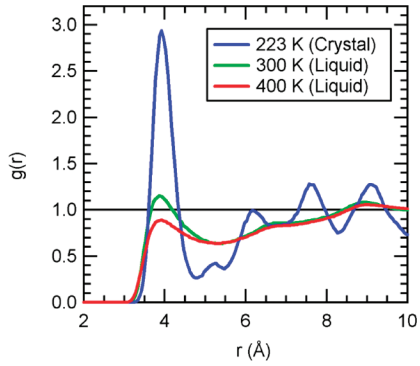

Figure 5. Radial distribution function $g(r)$ of intermolecular methyl−methyl distance derived from the crystal and liquid simulations at different temperatures.

In the RDF of the computed crystal lattice, the first peak appears at 3.9 Å, which compares well with the nearest intermolecular Me−Me distances in the experimental crystal,[19] which are distributed from 3.79 Å to 4.55 Å. Furthermore, there exist four additional peaks at 5.2 Å, 6.2 Å, 7.6 Å, and 9.1 Å, respectively, which reflect the highly ordered packing in the molecular crystal. In comparison, the first peaks of the RDFs of the liquid computed at 300 and 400 K are located near 3.9 Å, but the corresponding heights are considerably smaller than that of the computed crystal. Also, the RDFs of the liquid at these two temperatures show a loss of ordered structure above 5.0 Å.

It is worth mentioning that LJ parameters for methane and methyl groups have been developed by other authors as well. For instance, Jorgensen and co-workers[37] have developed LJ parameters for methane and CH_3 parameters for different hydrocarbons which are now part of the OPLS force field, while Steele[36] has proposed LJ parameters for methane which are extensively used in the literature. In principle, such parameter sets could be utilized in the simulation of OMCTS with eq 1 following our strategy (i.e., methyl site only). However, they are located in a zone of the penalty landscape corresponding to larger values of F (see Figure 3).

Finally, we also checked the anisotropy of the intermolecular potential (model-B) as applied to the OMCTS dimer. The potential curves corresponding to the interaction of OMCTS molecules with three different relative orientations, A−C, are plotted in Figure 6. Dimer C with the OMCTS molecules oriented face-to-face possesses the lowest energy (R = 6.0 Å, E_{min} = −3.69 kcal/mol), the methyl−methyl interactions being maximized. The second minimum is that of dimer A where the OMCTS molecular planes are coplanar to each other (R = 9.0 Å, E_{min} = −2.70 kcal/mol). The weakest binding is obtained for dimer B where the molecular planes of OMCTS are perpendicular to each other (R = 8.6 Å, E_{min} = −1.50 kcal/mol). This result is in line with the nonspherical (disk-like) shape of the OMCTS molecule. Hence, the development of such intermolecular potential seems meaningful for the atomistic study of this complex liquid.

V. Liquid Phase Simulation

In this section, we investigate the performance of Model-B. We performed a series of MD simulations to calculate the

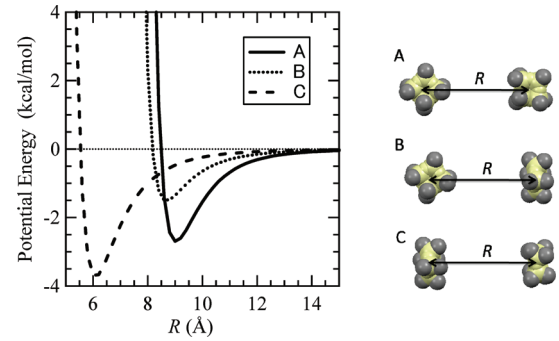

Figure 6. Potential curves of Model-B for three different configurations of the OMCTS dimer. The mean molecular planes of the two molecules are oriented as follows: A, coplanar; B, perpendicular; and C, parallel. The atoms of the siloxane ring define the mean molecular plane of OMCTS. R is the distance between the centers of mass. The relative orientation of OMCTS molecules is kept fixed during the scan.

temperature dependence of the density, diffusion coefficient, and shear viscosity of the liquid phase. The same type of simulation as the liquid case described in section III (with 216 molecules) was executed except that a longer total time step of 15 ns was used. In addition, for T = 300 and 400 K, we also tested a simulation box composed of 640 molecules so as to confirm that the calculated properties do not change when a larger system is employed. The diffusion coefficient D was derived using the Einstein relation (p 60 in ref 12):

$$D = \lim_{t\to\infty} \frac{1}{6Nt} \left\langle \sum_{i=1}^{N} [\mathbf{r}_i(t) - \mathbf{r}_i(0)]^2 \right\rangle \quad (4)$$

where $\mathbf{r}_i(t)$ is the center of mass position vector of molecule i at time t and N is the number of molecules in the simulation cell. The quantity in brackets $\langle ... \rangle$ indicates an ensemble average, and here it means taking the average value over different time origins for each time interval t. The shear viscosity η was calculated by the following equation:[38]

$$\eta = \lim_{t\to\infty} \frac{V}{20k_B Tt} \sum_{\alpha=x,y,z} \sum_{\beta=x,yz} \langle [L^{\alpha\beta}(t) - L^{\alpha\beta}(0)]^2 \rangle \quad (5)$$

where k_B is the Boltzmann constant and V is the volume of the system. $L^{\alpha\beta}$ is defined as

$$L^{\alpha\beta}(t) = \int_0^t P^{\alpha\beta}(\tau)\, d\tau \quad (6)$$

and P is the traceless symmetric part of the stress tensor σ:

$$P^{\alpha\beta} = \frac{\sigma^{\alpha\beta} + \sigma^{\alpha\beta}}{2} - \frac{\delta^{\alpha\beta}}{3} \sum_{\gamma=x,y,z} \sigma^{\gamma\gamma} \quad (7)$$

where $\delta^{\alpha\beta}$ =1 for $\alpha = \beta$ and 0 for $\alpha \neq \beta$. The stress tensor was calculated as

$$\sigma^{\alpha\beta} = \frac{1}{V}\left[\sum_{i=1}^{N} \sum_{a\in i} m_a v_a^\alpha v_a^\beta + \sum_i \sum_{j>i} \sum_{a\in i} \sum_{b\in j} (r_a^\alpha - r_b^\alpha) \frac{\partial U}{\partial (r_a^\beta - r_b^\beta)} \right] \quad (8)$$

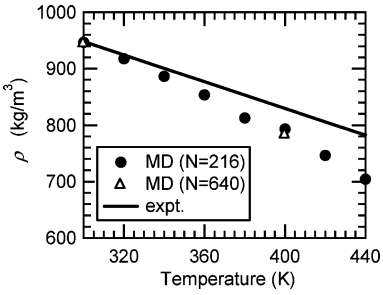

Figure 7. Temperature dependence of liquid density, ρ. Experimental curve, $\rho = 1303.79-1.18562T$, taken from Palczewska-Tulińska and Oracz.[33] N is the number of molecules in the simulation box.

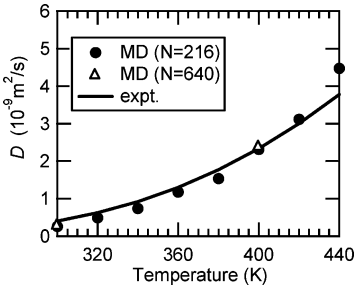

Figure 8. Temperature dependence of diffusion coefficient, D. Experimental curve, $D = 10^9 \exp(-14.599-2110/T)$, taken from Fischer and Weiss.[40] N is the number of molecules in the simulation box.

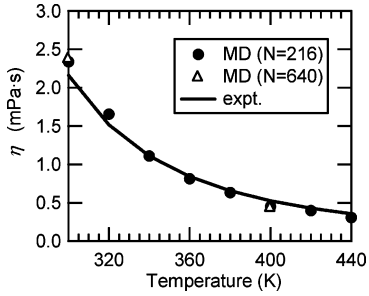

Figure 9. Temperature dependence of shear viscosity, η. Experimental curve, $\eta = -4.8920 + 1698.7/T$, taken from Palczewska-Tulińska and Oracz.[33] N is the number of molecules in the simulation box.

where U is the potential energy of the system and m_i, r_a^{α}, and v_a^{α} are the mass, coordinate, and velocity of atom a, respectively. The subscript $a \in i$, means the summation on a is taken over molecule i.

Equation 5 is the Einstein form of the Green-Kubo relation and is based on the relation derived by Daivis and Evans[39] for an isotropic system:

$$\frac{V}{k_B T} \sum_{\alpha=x,y,z} \sum_{\beta=x,y,z} \int_0^{\infty} \langle P^{\alpha\beta}(t) P^{\alpha\beta}(0) \rangle \, dt = 10\eta \qquad (9)$$

This relation makes it possible to use all the components of the stress tensor, including the diagonal ones, in the calculation of η to enhance the statistical reliability.

The liquid properties computed in the range 300−440 K are compared against the experimental results in Figures 7−9. Figure 7 compares the calculated liquid density (ρ) against the experimental values obtained from ref 33. The agreement between calculated and experimental liquid densities is quite good in the low-temperature region around 300 K but degrades by increasing the temperature at above 400 K. Actually, most of the parameter sets tested in the empirical refinement stage underestimated experimental liquid density at 400 K, thus suggesting that additional parameters would be needed to improve this situation. However, the maximum relative error is about 10% (at 440 K), which is good enough if one thinks of the simplicity of the present model, while adding more parameters would make the model computationally less efficient. One possible explanation for the observed deviation of ρ could be related to the rigid body approximation employed here for OMCTS whereas a flexible molecule would better optimize packing.

Figure 8 compares the calculated diffusion coefficient (D) against the experimental data from ref 40. The overall agreement with the experiment is good in the whole temperature range of 300−440 K, though the calculated diffusion coefficient increases slightly in the high temperature region. This corresponds to a lower density at these temperatures. Figure 9 compares the calculated shear viscosity (η) against the experimental data taken from ref 33. The agreement with experiments is good, though the calculated η is slightly higher in the low temperature region and lower at the high temperature region. It is noted that the diffusion coefficient and shear viscosity were not included in the parameter optimization process, which again supports that the model correctly captures the essential physics of the intermolecular interaction within liquid OMCTS.

VI. Conclusions

We developed a new atomistic potential model for the molecular simulation of OMCTS. We could simplify the potential on the assumption that the dominant part of intermolecular interaction in OMCTS is the interaction among methyl groups, as observed in the molecular crystal. Following this approach, the present model possesses only two parameters thereby making it possible to perform an efficient empirical refinement of the potential using the experimental data of both the crystal and liquid phases. Our new model successfully reproduces both the crystal lattice constants and liquid transport properties of OMCTS in a wide range of temperatures, thereby making the large scale atomistic simulation of this molecular liquid possible.

Acknowledgment. This research is supported by the Core Research for Evolutional Science and Technology (CREST) program of the Japan Science and Technology Agency (JST). We thank Dr. Bill Smith (Daresbury Laboratory) and the CCP-5 project for a copy of the DL_POLY molecular simulation package. The comments of anonymous reviewers are gratefully acknowledged.

Supporting Information Available: A table containing the calculated properties and penalty function F for all the $\varepsilon-\sigma$ pairs explored in this study; a table containing the translational and the first and second order rotational correlation times, τ_v, τ_{R1}, and τ_{R2} for the liquid phase simulation with Model-B; and the Cartesian coordinates of our rigid-

body OMCTS model. This material is available free of charge via the Internet at http://pubs.acs.org.

References

(1) Horn, R. G.; Israelachvili, J. N. *J. Chem. Phys.* **1981**, *75*, 1400–1411.

(2) Israelachvili, J. N. *Intermolecular and Surface Forces*, 2nd ed.; Academic Press: London, 1992.

(3) Klein, J.; Kumacheva, E. *J. Chem. Phys.* **1998**, *108*, 6996–7009.

(4) Demirel, A. L.; Granick, S. *J. Chem. Phys.* **2001**, *115*, 1498–1512.

(5) Kurihara, K. *Prog. Colloid Polym. Sci.* **2002**, *121*, 49–56.

(6) Mizukami, M.; Kusakabe, K.; Kurihara, K. *Prog. Colloid Polym. Sci.* **2004**, *128*, 105–108.

(7) Sakuma, H.; Otsuki, K.; Kurihara, K. *Phys. Rev. Lett.* **2006**, *96*, 046104.

(8) Somers, S. A.; Ayappa, K. G.; McCormick, A. V.; Davis, H. T. *Adsorption* **1996**, *2*, 33–40.

(9) Su, Z.; Cushman, J. H.; Curry, J. E. *J. Chem. Phys.* **2003**, *118*, 1417–1422.

(10) Ayappa, K. G.; Mishra, R. K. *J. Phys. Chem. B* **2007**, *111*, 14299–14310.

(11) Allen, M. P.; Tildesley, D. J. *Computer Simulation of Liquids*; Oxford University Press: New York, 1987.

(12) Haile, J. M. *Molecular Dynamics Simulation: Elementary Methods*; Wiley: New York, 1992.

(13) Stone, A. J. *Science* **2008**, *321*, 787–789.

(14) McCarty, J.; Lyubimov, I. Y.; Gruenza, M. G. *J. Phys. Chem. B* **2009**, *113*, 11876–11886.

(15) Murtola, T.; Bunker, A.; Vattulainen, I.; Deserno, M.; Karttunen, M. *Phys. Chem. Chem. Phys.* **2009**, *11*, 1869–1892.

(16) (a) Lopez, C. F.; Nielsen, S. O.; Srinivas, G.; DeGrado, W. F.; Klein, M. L. *J. Chem. Theory Comput.* **2006**, *2*, 649–655. (b) DeVane, R.; Shinoda, W.; Moore, P. B.; Klein, M. L. *J. Chem. Theory Comput.* **2009**, *5*, 2115–2124.

(17) Spieser, S. A. H.; Leeflang, B. R.; Kroon-Batenburg, L. M. J.; Kroon, J. *J. Phys. Chem. A* **2000**, *104*, 7333–7338.

(18) Peguin, R. P. S.; Kamath, G.; Potoff, J. J.; da Rocha, S. P. *J. Phys. Chem. B* **2009**, *113*, 178–187.

(19) Steinfink, H.; Post, B.; Fankuchen, I. *Acta Crystallogr.* **1955**, *8*, 420–424.

(20) Møller, C.; Plesset, M. S. *Phys. Rev.* **1955**, *46*, 618–622.

(21) Ditchfield, R.; Hehre, W. J.; Pople, J. A. *J. Chem. Phys.* **1971**, *54*, 724–728.

(22) McLean, A. D.; Chandler, G. S. *J. Chem. Phys.* **1980**, *72*, 5639–5348.

(23) Dunning, T. H., Jr. *J. Chem. Phys.* **1989**, *90*, 1007–1023.

(24) Frisch, M. J.; Trucks, G. W.; Schlegel, H. B.; Scuseria, G. E.; Robb, M. A.; Cheeseman, J. R.; Montgomery, J. A., Jr.; Vreven, T.; Kudin, K. N.; Burant, J. C.; Millam, J. M.; Iyengar, S. S.; Tomasi, J.; Barone, V.; Mennucci, B.; Cossi, M.; Scalmani, G.; Rega, N.; Petersson, G. A.; Nakatsuji, H.; Hada, M.; Ehara, M.; Toyota, K.; Fukuda, R.; Hasegawa, J.; Ishida, M.; Nakajima, T.; Honda, Y.; Kitao, O.; Nakai, H.; Klene, M.; Li, X.; Knox, J. E.; Hratchian, H. P.; Cross, J. B.; Bakken, V.; Adamo, C.; Jaramillo, J.; Gomperts, R.; Stratmann, R. E.; Yazyev, O.; Austin, A. J.; Cammi, R.; Pomelli, C.; Ochterski, J. W.; Ayala, P. Y.; Morokuma, K.; Voth, G. A.; Salvador, P.; Dannenberg, J. J.; Zakrzewski, V. G.; Dapprich, S.; Daniels, A. D.; Strain, M. C.; Farkas, O.; Malick, D. K.; Rabuck, A. D.; Raghavachari, K.; Foresman, J. B.; Ortiz, J. V.; Cui, Q.; Baboul, A. G.; Clifford, S.; Cioslowski, J.; Stefanov, B. B.; Liu, G.; Liashenko, A.; Piskorz, P.; Komaromi, I.; Martin, R. L.; Fox, D. J.; Keith, T.; Al-Laham, M. A.; Peng, C. Y.; Nanayakkara, A.; Challacombe, M.; Gill, P. M. W.; Johnson, B.; Chen, W.; Wong, M. W.; Gonzalez, C.; Pople, J. A. *Gaussian 03, Revision D.02*; Gaussian, Inc.: Wallingford, CT, 2004.

(25) Li, A. H.-T.; Chao, S. D. *J. Mol. Struct. (Theochem)* **2009**, *897*, 90–94.

(26) Cramer, C. J. *Essentials of Computational Chemistry: Theories and Models*, 2nd ed.; Wiley: Chichester, 2005.

(27) Boys, S. F.; Bernardi, F. *Mol. Phys.* **1970**, *19*, 553–566.

(28) Smith, W. *Mol. Simul.* **2006**, *32*, 933–933.

(29) Berendsen, H. J. C.; Postma, J. P. M.; van Gunsteren, W. F.; DiNola, A.; Haak, J. R. *J. Chem. Phys.* **1984**, *81*, 3684–3690.

(30) Miller III, T. F.; Eleftheriou, M.; Pattnaik, P.; Ndirango, A.; Newns, D. *J. Chem. Phys.* **2002**, *116*, 8649–8659.

(31) Hunter, M. J.; Hyde, J. F.; Warrick, E. L.; Fletcher, H. J. *J. Am. Chem. Soc.* **1946**, *68*, 667–672.

(32) Osthoff, R. C.; Grubb, W. T.; Burkhard, C. A. *J. Am. Chem. Soc.* **1953**, *75*, 2227–2229.

(33) Palczewska-Tulińska, M.; Oracz, P. *J. Chem. Eng. Data* **2005**, *50*, 1711–1719.

(34) Mayo, S. L.; Olafson, B. D.; Goddard, W. A. *J. Phys. Chem.* **1990**, *94*, 8897–8909.

(35) Smith, J. S.; Borodin, O.; Smith, G. D. *J. Phys. Chem. B* **2004**, *108*, 20340–20350.

(36) Steele, W. A. *The Interaction of Gases with Solid Surfaces*, 1st ed.; Pergamon Press: Oxford, 1974; p 56.

(37) Jorgensen, W. L.; Madura, J. D.; Swenson, C. J. *J. Am. Chem. Soc.* **1984**, *106*, 6638–6646.

(38) Mondello, M.; Grest, G. S. *J. Chem. Phys.* **1997**, *106*, 9327–9336.

(39) Daivis, P. J.; Evans, D. J. *J. Chem. Phys.* **1994**, *100*, 541–547.

(40) Fischer, J.; Weiss, A. *Ber. Bunsen—Ges. Phys. Chem.* **1986**, *90*, 896–905.

CT9006053